BEATA FIGARSKA-WARCHOŁ[1], MAREK REMBIŚ[2]

Transformations of diatomite components and changes in its technical properties caused by calcination at different temperatures – a case study of the Jawornik deposit, Poland

Introduction

The formation of diatomite rocks may be related to various environmental conditions: shallow and deep sea, as well as freshwater lakes (usually of volcanic origin) and brackish coastal lakes (Bradbury and Krebs 1995; Plunkett et al. 2004; Harwood et al. 2007; Opfergelt et al. 2011; Vassileva et al. 2011; Flower 2013; Frings et al. 2014; Smirnov et al. 2017; Zahradnik et al. 2019). Sedimentation conditions had a significant impact on the chemical composition and physical-mechanical properties of these rocks, determining the possibility of their industrial use. On world markets, diatomite raw materials are offered mainly by the

---

✉ Corresponding Author: Beata Figarska-Warchoł; e-mail: figarska@agh.edu.pl

[1] AGH University of Krakow, Poland; Mineral and Energy Economy Research Institute PAS, Kraków, Poland; ORCID iD: 0000-0002-6962-1775; e-mail: figarska@agh.edu.pl

[2] AGH University of Krakow, Poland; ORCID iD: 0000-0003-2879-3949; Scopus ID: 25028717400; e-mail: rembis@agh.edu.pl

United States. Denmark, China, Turkey, Argentina, Mexico, and Peru play a much smaller role, and mining in 19 other countries worldwide is of minor importance (Crangle 2024). In Poland, diatomite rocks occur in the eastern part of the Polish Outer Carpathians (between the Wisłok River and Przemyśl) in the profile of Oligocene–Lower Miocene flysch deposits of the Skole Unit, where they form three separate complexes. They differ in terms of lithology and thickness of rock formations, containing several varieties of diatomite rocks with different colors, compactness, clay and sand content, degree of silicification, as well as other shapes of fragments into which the rock breaks down during weathering (Russocki 1981; Kotlarczyk et al. 1986; Kotlarczyk 1988a, b; Figarska-Warchoł et al. 2015). Diatomite rocks are mainly represented by siliceous-clayey rocks of very low density, usually homogeneous and with a varying share of diatom shells or, more often, their crushed fragments (detritus), as well as grains of quartz, feldspar, glauconite, and mica, bonded with a siliceous-clay cement. A characteristic and usually most desirable feature of diatomite rocks is their high open porosity and a large amount of silica. The average diatomite raw material from Poland has a chemical composition and technical properties similar to other diatomites of marine origin. Open porosity of 22–42%, a specific surface area of 12–16 m^2/g, and SiO_2 content of 61–84% favour the use of this material already in its raw state as a sorption and filtration material (Kotlarczyk 2008), and a lesser extent also for the production of aggregates. Some world diatomites originating from, for example, China, Czechia, Bulgaria, Russia, Thailand, the USA, Bolivia, and Turkey are characterised by similar quality (Behl 1999; Goren et al. 2002; Zhi-Ying et al. 2009; Vassileva et al. 2011, 2013; Posi et al. 2014; Smirnov et al. 2017; Zahradník et al. 2019) and are commonly subjected to technological processes aimed at improving their quality. Modification of the technical parameters of diatomite rocks can be carried out using various methods, depending on their initial properties and the expected final effect. The most frequently used processes include thermal calcination and chemical modification. The advantage of calcination is the lack of need to create a complicated technical installation. Its essential part is a furnace that allows diatomite to be calcined at a given temperature. Both diatomite aggregate and ground powder of this rock material can be subjected to this process.

Calcination of diatomite raw material from Poland and research on the effects of this process have been performed and described previously (Figarska-Warchoł et al. 2019, Marczyk et al. 2022). These studies showed various changes in porosity, macropores, specific surface area, and strengthening of the rock structure in various varieties of diatomite rocks subjected to calcination. Less attention was paid to changes in the mineral composition and structure of diatomites caused by calcination at gradually increasing temperatures and how this process influenced the technical properties of the obtained product. These issues are the subject of this work. The research concerned a variety of relatively widespread, dark grey diatomite with blocky disintegration, occurring in beds several meters high and representing an average quality raw material.

1. Materials

The research material was collected from the only active diatomite deposit in Poland - Jawornik, located in the Polish part of the Flysch Carpathians within the Skole Unit. It is composed of layers belonging to the youngest flysch formations from the Paleogene–Neogene boundary, including the Lower Miocene member of the Leszczawka Diatomite Member (Koszarski and Żytko 1961; Kotlarczyk 1966, 1982; Kotlarczyk and Kaczmarska 1987). These formations originate from the final stage of the synorogenic closing of sedimentary basins in the Polish part of the Flysch Carpathians, which was accompanied by volcanic activity (Malata and Poprawa 2006; Oszczypko 2008; Szydło et al. 2014). They are the result of redeposition of detrital material from other parts of the basin as a result of mudflows and submarine landslides (Kotlarczyk 1982). Conditions of sedimentation influenced the diverse petrographic composition of these rocks. A detailed description of the lithological varieties of diatomites occurring in the deposit was presented in the work of Figarska-Warchoł et al. (2015). The test samples came from a uniform layer several meters thick and represented a variety of blocky, dark beige diatomites (variety BD) with average properties both in the scale of this deposit and in general for diatomites from the Leszczawka syncline.

2. Methods

A homogeneous block of rock was used to prepare nine three-piece sets of samples with irregular shapes and a volume of approximately 50 cm^3 each. Each set was calcined at a different temperature (300°C, 400°C, 500°C, 600°C, 700°C, 800°C, 900°C, 1,000°C or 1,200°C) in the ambient air. The temperature of the laboratory furnace was initially increased at a rate of 20ºC/min. in the range of 20–150ºC, and then at a rate of 4ºC/min. to reach the target, previously determined calcination temperature, which was maintained for 24 h. The samples were cooled to room temperature for 48 hours before being removed from the oven.

Laboratory tests of diatomites began with the analysis of the petrographic characteristics of the rock raw material, obtained in the previous work (Figarska-Warchoł et al. 2015), based on the results of the chemical composition tests of powdered samples using the ICP-OES method and the loss on ignition determined for the sample previously dried at 105±5°C. The petrographic description was performed during macroscopic observations of samples and analysis of thin sections in a transmitted light microscope, and then using a scanning electron microscope (SEM) FEI Quanta 200 FEG (low-vacuum) with a BSE detector coupled to an EDS analyser with low vacuum conditions. The EDS analysis was performed without a pattern using the EDAX system.

Changes in the mineral composition, as well as the structure and texture of diatomites, occurring under the influence of temperature, were first assessed based on the results of thermal analysis of raw diatomite samples and X-ray diffraction tests of raw and calcined diatomite samples, and then by performing SEM observations of thin sections. Thermal

analysis was conducted in ambient air using a NETZSCH STA 449 F3 thermal analyser with Al_2O_3 crucible. This allowed for the measurement of mass changes (TG, DTG) and thermal effects (DTA) in the temperature range of 30–980°C. XRD analyses were carried out using a DRON 3.0 X-ray diffractometer with CuKα radiation and the Debye-Sherrer powder method. Scanning was made in the range of 2–70° 2θ in 0.05° 2θ steps.

For each diatomite sample in the raw state and after thermal modification, measurements of basic physical properties were carried out, i.e. apparent density (ρo) and water absorption (Ab) according to the standards EN 1936 and EN 13755, respectively. Transformations of mineral components and changes in the structure of the rock-influenced its mechanical strength, which was assessed by performing Vickers microhardness measurements of raw and calcined samples. The Vickers hardness HV expresses the resistance of a rock to pressing a pyramidal diamond indenter and is calculated using the load exerted by the indenter and the average diagonal of the square-shaped indentation mark. The measurements were conducted using a Testlab HVKD1000IS hardness tester. About a relatively low hardness of samples, a minimum available load of 2.942 N (0.3 kgf) of indenter was applied. The average hardness value for each sample was calculated based on the results obtained from 20 indentations made along the marked line.

3. Results

3.1. Petrographic characteristics of raw diatomite

The raw diatomite used in the research represented a dark beige or grey-brown siliceous rock, with an apparent density of approximately 1.34 g/cm^3, which easily disintegrates under the impact of a hammer into smaller fragments with quite regular block-like shapes. Diatomite of this variety has a fine-detrital texture and usually chaotic structure, sometimes varied by the presence of diffusion Liesegang rings developed near the surface of the discontinuities covered with rusty crusts of iron compounds. The smallest rock components were not macroscopically distinguishable. Microscopic observations allowed us to conclude that the granular components are dominated by whole or, more often, crushed, opal diatom shells, usually with elongated or round shapes (41.2% by volume of the rock) (Figure 1) and sizes of 5–90 μm, sometimes up to 50–100 μm. There are smaller amounts of quartz grains (6.8% by volume of the rock) of various sizes, and rarely mica plates (2.6%), feldspar grains (1.6%), glauconite concretions (0.8%) (Table 1), and occasionally ilmenite or titanite grains (the latter not visible during quantitative determinations).

Based on the results of microscopic petrographic analysis (Table 1) and chemical analysis (Table 2), described in the previous article (Figarska-Warchoł et al. 2015), the content of groundmass components was estimated. The above-mentioned grains are surrounded by a silica-clay mass of the matrix type (47.0% by volume of the rock), containing approxi-
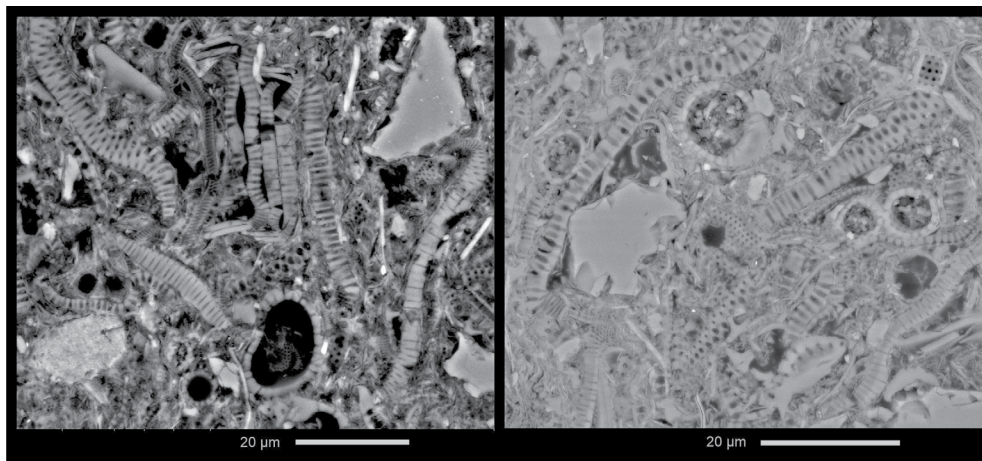
Fig. 1. SEM images of thin sections of A) raw diatomite (left)
and B) diatomite calcined at 400°C (right)

Rys. 1. Obraz w mikroskopie SEM płytki cienkiej diatomitu A) surowego (po lewej)
i B) kalcynowanego w temp. 400°C (po prawej)

Table 1.   Mineral composition (vol. %) of the tested diatomite (Figarska-Warchoł et al. 2015)

Tabela 1.   Skład mineralny (udział obj.) badanego diatomitu

Diatoms	Quartz	Micas	Feldspars	Glauconite	Groundmass			
41.2%	6.8%	2.6%	1.6%	0.8%	47.0%			
					estimated content of groundmass components			
					opal-A/ /opal-CT	clay minerals	(oxy-) hydroxide phases of iron	organic substance
					22–27%	21–29%	≈2%	≈5%

Table 2.   Chemical composition (wt %) of the tested diatomite (Figarska-Warchoł et al. 2015)

Tabela 2.   Skład chemiczny (% wag.) badanego diatomitu

SiO_2	Al_2O_3	$Fe_2O_3(T)$	MnO	MgO	CaO	Na_2O	K_2O	TiO_2	P_2O_5	LOI
78.74%	8.48%	2.96%	0.01%	0.62%	0.32%	0.28%	1.28%	0.35%	0.02%	7.66%

mately equal parts silica and clay minerals, represented mainly by illites and minerals from the smectite group. The silica component of the matrix is mainly opal-A, which forms very small fragments of diatoms (less than 2.5 micrometers), and less often opal-CT, which is the effect of recrystallization. The minor components of the groundmass are organic matter and iron oxides/hydroxides (Table 1), influencing, among others, the colour of diatomite.

The presence of the above-mentioned components affects the large proportion of 1,200 in the chemical composition of the rock (approx. 79%) and the smaller proportion of Al_2O_3 (approx. 8.5%) and Fe_2O_3 (approx. 3%) (Table 2). The loss on ignition is approximately 7.5% (Figarska-Warchoł et al. 2015).

3.2. DTA and XRD tests

Thermal analysis performed for raw diatomite showed a continuous loss of sample mass up to a temperature of 980°C, characterised by the highest intensity up to a temperature of approximately 300°C (Figure 2). This process was enhanced again in the range of approximately 450–500°C. The total weight loss reached approximately 11%. The DTA diagram shows the predominance of endothermic reactions during calcination in the temperature range of 30–980°C with a maximum of approximately 600–650°C. Exothermic reactions prevailed in the approximate range of 250–400°C.

Identification of mineral phases in the raw diatomite based on X-ray powder diffraction (XRD) showed mainly the presence of amorphous silica, as well as quartz, clay minerals, mica and feldspar (Figure 3). The first significant changes caused by calcination are marked in the diffractograms of samples exposed to temperatures of 400–500°C, mainly as a decrease in the smectite peaks (2θ in the range of 5–9°) and the disappearance of the kaolinite
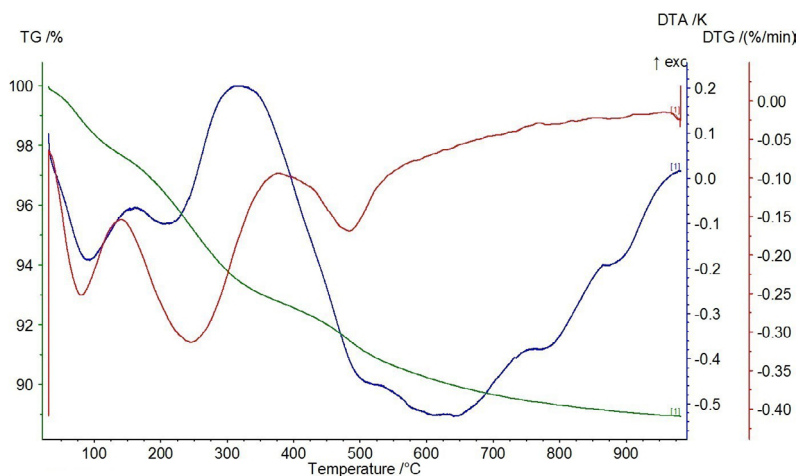

Fig. 2. DTA/TG/DTG thermal curves of the tested diatomite

Rys. 2. Krzywe termiczne DTA/TG/DTG badanego diatomitu

peak (2θ = 12.4°). At higher temperatures, the peaks corresponding to illite, muscovite, and feldspar decrease until they disappear at 900°C. At a temperature of 1,000°C, the share of the amorphous phase increases as well as hematite and cristobalite peaks appear. At the highest temperature (1,200°C) all of the amorphous silica phase is transformed into cristobalite. Moreover, the composition of diatomite exposed to this highest temperature also includes quartz, mullite, and hematite. In the case of quartz, only the main peaks are visible in the XRD diagram.
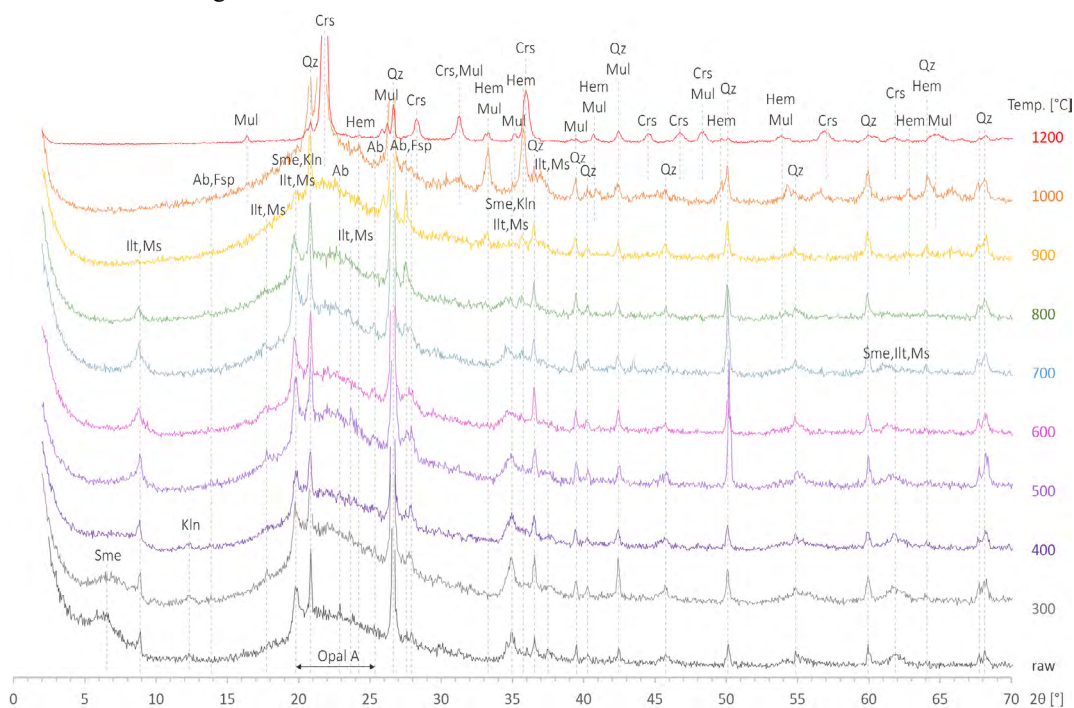

Fig. 3. X-ray diffractograms of diatomite samples calcined at different temperatures
Ab – albite, Crs – cristobalite, Fsp – feldspar, Hem – hematite, Ilt – illite, Kln – kaolinite,
Mul – mullite, Ms – muscovite, Qz – quartz

Rys. 3. Dyfraktogramy prób diatomitu kalcynowanego w różnych temperaturach

3.3. Analysis of SEM images

Thin sections of diatomites calcined at various temperatures were analysed using a scanning electron microscope (Figure 4–10). The changes occurring within diatoms were observed, paying particular attention to the smallest pores, the disappearance of which accompanies the process of silica melting (Figure 4). Grains of quartz (Figure 5), feldspar (Figure 6), ilmenite (Figure 7), titanite as well as mica flakes (Figure 8), glauconite pellets (Figure 9) and clay-silica matrix were also studied.
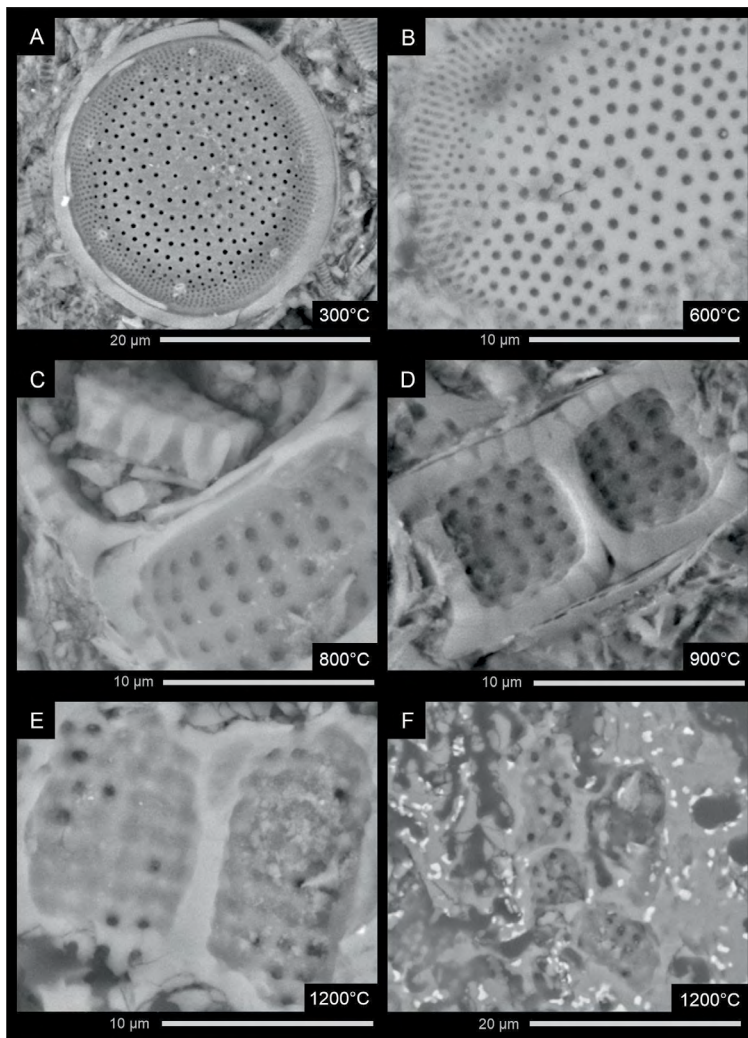
Fig. 4. SEM images of diatoms in samples of diatomite calcined at various temperatures

Rys. 4. Obrazy SEM okrzemek w próbach diatomitu kalcynowanego w różnych temperaturach

The SEM images do not show any transformations of the rock components caused by calcination at low temperatures (up to 300°C) (Figure 4A, 5A, 6A, 8A, 9A). The earliest reaction to temperature, the effects of which could be observed under a microscope, was demonstrated by feldspar grains. Its first signs were noticed at a temperature of 600°C in the form of irregular cracks in these minerals (Figure 6B). At that time, the structure of some opal diatoms and quartz grains also began to change (small cracks appeared) (Figure 4B). At a temperature of 900°C, most of the rock components were significantly transformed,
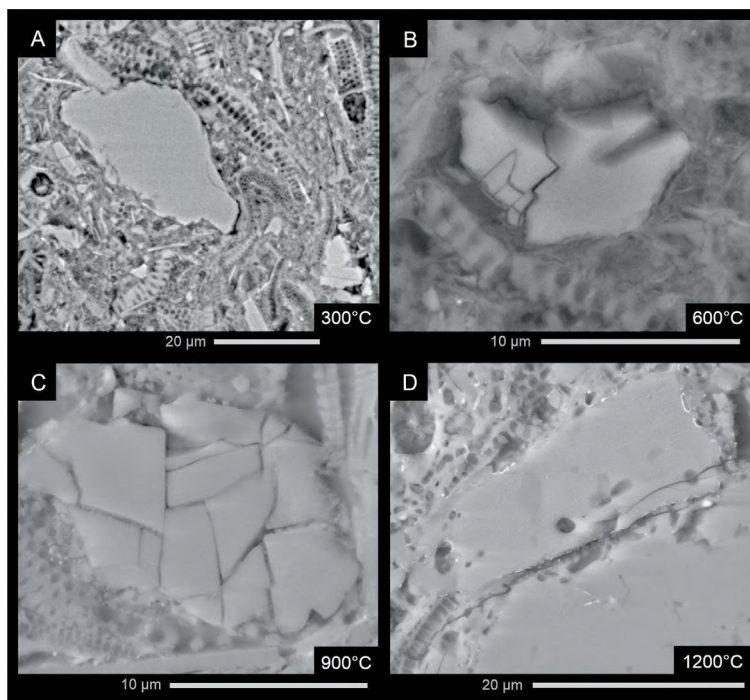
Fig. 5. SEM images of quartz grains in samples of diatomite calcined at various temperatures

Rys. 5. Obrazy SEM ziaren kwarcu w próbach diatomitu kalcynowanego w różnych temperaturach

and the highest calcination temperature – 1,200°C – led to a significant loss of the original diatomite structure. A detailed description of the changes observed under the microscope was presented in the Discussion section.

3.4. Changes in the physical and mechanical properties of diatomite

Changes in the mineral composition and structure of diatomites exposed to high temperatures were expressed in the modification of their physical properties. Macroscopically, the colour change of the samples was noticeable (Figure 11). As a result of calcination, the raw dark beige diatomite initially turned dark grey at 300°C, lightening up to 700°C, while the Liesegang rings still retained their yellow-brown colour. At higher temperatures, the samples became increasingly rusty-red throughout their volume. The heating process at 1,200°C ended with the diatomite turning almost purple. Calcination at each stage promoted the formation of fractures in the samples, most intensely after reaching the temperature of 1,000°C.
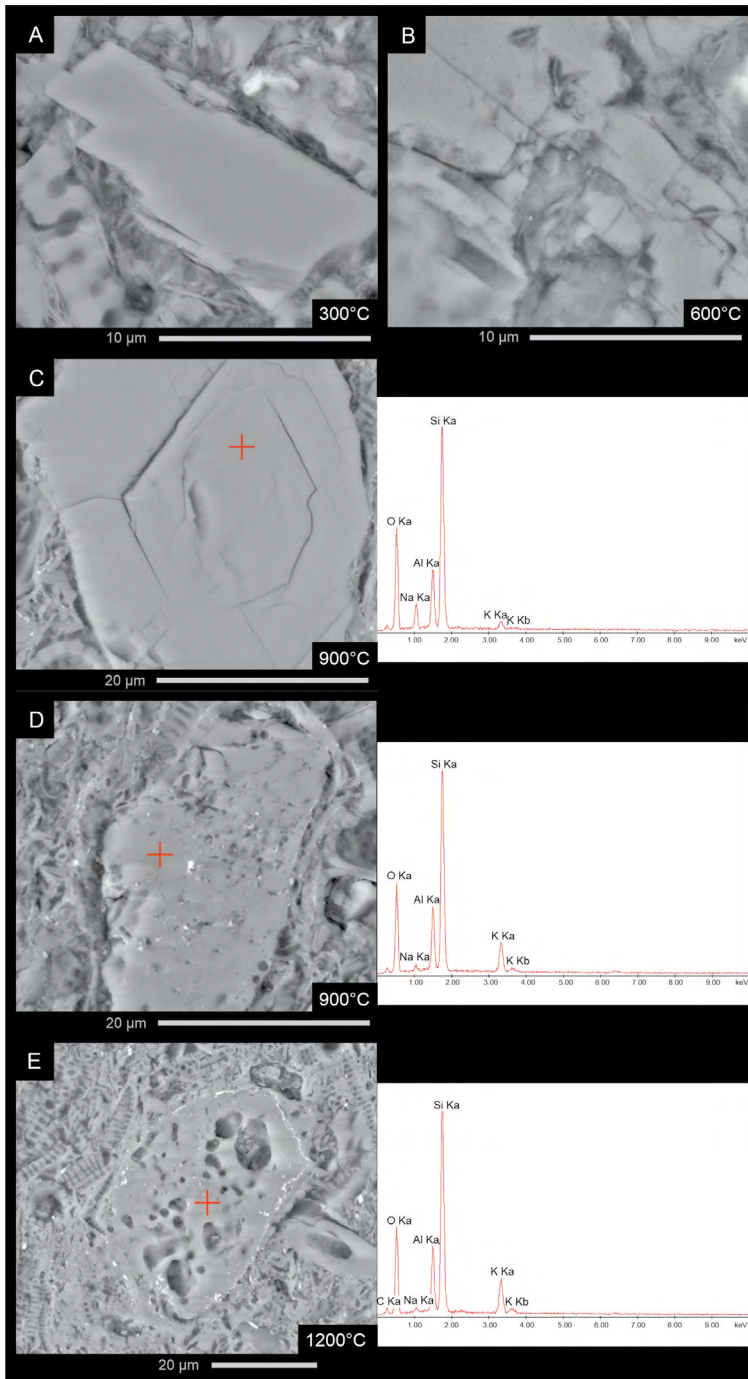
Fig. 6. SEM images of feldspar grains in samples of diatomite calcined at various temperatures

Rys. 6. Obrazy SEM ziaren skaleni w próbach diatomitu kalcynowanego w różnych temperaturach
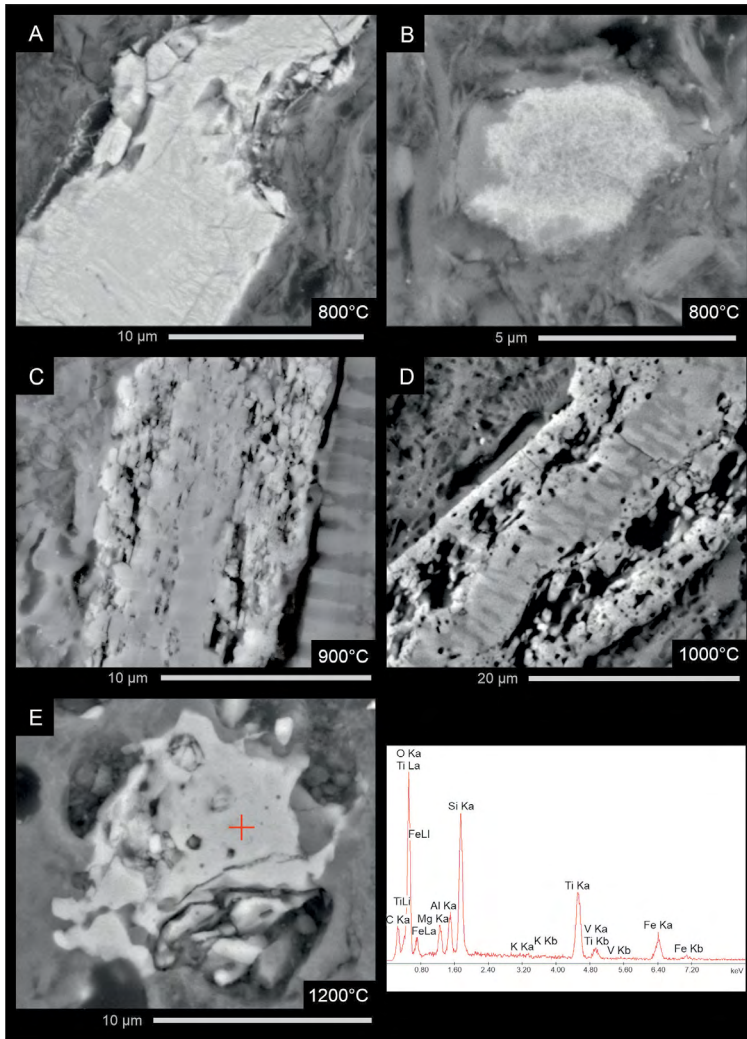
Fig. 7. SEM images of the stages of ilmenite grain decomposition at increasing calcination temperatures

Rys. 7. Obrazy SEM etapów dekompozycji ziaren ilmenitu w narastających temperaturach kalcynacji

Samples of raw diatomites were characterised by apparent density in the range of 1.32––1.38 g/cm^3 (average 1.34 g/cm^3) and water absorption in the range of 23.77–27.02% (average 25.20%). The pore space of diatomite was observed under an optical and electron microscope. It is composed of numerous pores present both inside the diatom frustules and between the grains (Figure 1). Diatomites of the BD variety (dark beige and blocky), which included the samples used in the research, were characterised by the presence of many pore bottlenecks, which made quite a large part of the pores inaccessible to capillary water. This
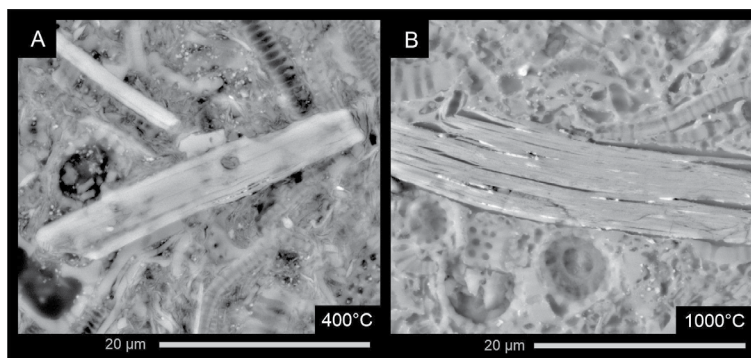
Fig. 8. SEM images of mica flakes in samples of diatomite calcined at various temperatures

Rys. 8. Obrazy SEM łusek miki w próbach diatomitu kalcynowanego w różnych temperaturach

Table 3.   Physical and mechanical properties of raw and calcined diatomites

Tabela 3.   Właściwości fizyczno-mechaniczne surowego i kalcynowanego diatomitu

| Calcination temperature (°C)	Apparent density (g/cm^3)	Water absorption (%)	Open porosity (%)	Vickers hardness $HV_{0.3}$ (MPa)	Relative changes in $HV_{0.3}$ compared to raw diatomite (%)
0	1.34 1.32–1.38	25.20 23.77–27.02	33.86 31.55–35.73	13.56 12.15–15.91	–
300	1.30 1.296–1.299	27.89 27.80–27.99	36.20 36.11–36.28	13.54 11.78–15.51	–0.15
400	1.29 1.27–1.31	29.21 28.64–29.78	37.77 37.56–37.97	14.25 11.02–19.20	5.09
500	1.27 1.27–1.28	29.34 29.22–29.46	37.36 37.10–37.62	18.39 14.79–21.73	35.62
600	1.27 1.269–1.272	29.63 29.57–29.70	37.65 37.52–37.78	20.80 13.95–26.64	53.39
700	1.28 1.27–1.29	28.54 28.01–29.06	36.45 36.06–36.84	22.68 19.74–26.73	67.26
800	1.27 1.25–1.29	28.90 27.97–29.84	36.68 35.99–37.38	27.49 22.21–34.06	102.73
900	1.28 1.27–1.30	29.37 28.45–30.28	37.61 36.85–38.38	51.00 37.42–78.37	276.11
1,000	1.47 1.45–1.49	23.18 22.51–23.85	34.11 33.59–34.62	79.24 49.76–129.43	484.37
1,200	1.65 1.61–1.70	12.94 11.43–14.46	21.31 19.40–23.23	85.65 60.66–144.68	532.01
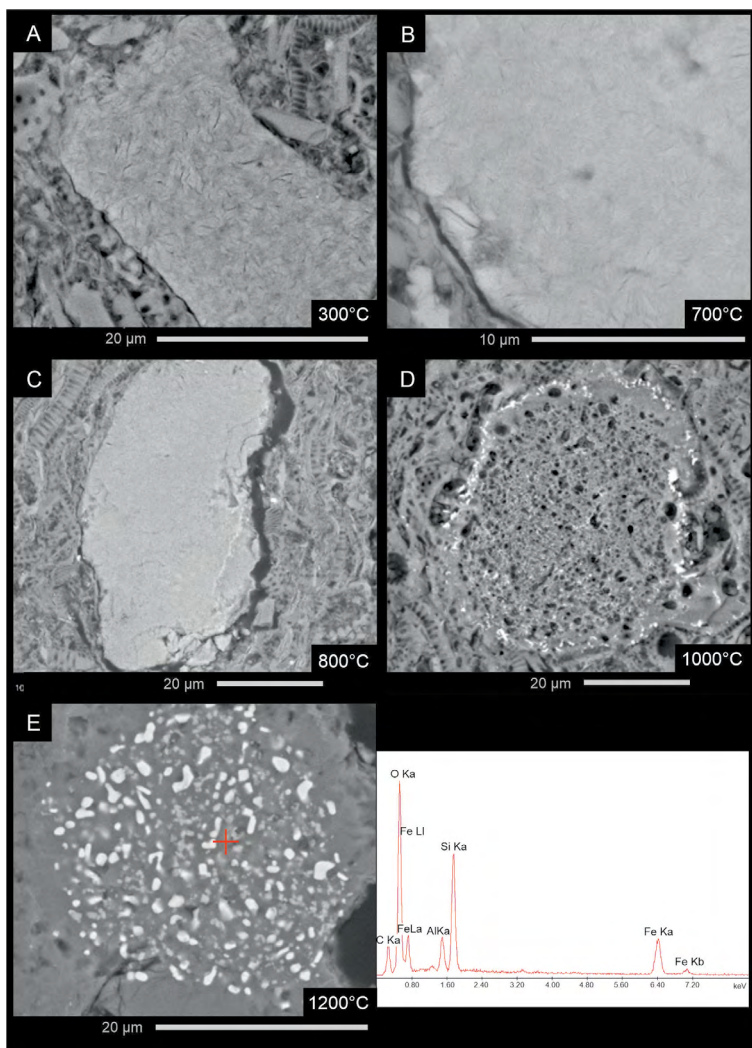
Fig. 9. SEM images of glauconite pellets in diatomite calcined at various temperatures

Rys. 9. Obrazy SEM skupień glaukonitu w diatomicie kalcynowanym w różnych temperaturach

is evidenced by the large difference between the total open porosity (33.65–38.79%, average 36.60%) measured with a mercury porosimeter (Figarska-Warchoł et al. 2015) and the open porosity (31.55–35.73%, average 33.86%) determined by the method described in EN 1936 standard (Table 3).

The calcination process at temperatures below 400°C increased the water absorption and open porosity to 29.21 and 37.77%, respectively (Table 3). These parameters remained at a similar level until the temperature of 900°C, and then decreased significantly to 12.94%
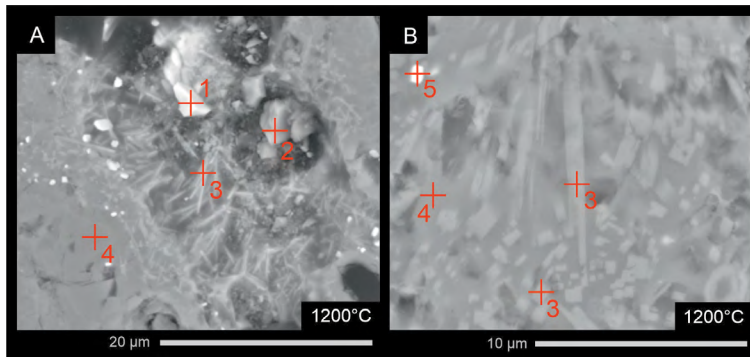
Fig. 10. SEM images of mineral phases present in diatomite calcined at 1,200°C
1 – remnant of ilmenite, 2 – quartz, 3 – mullite, 4 – remnants of K-feldspar, 5 – hematite

Rys. 10. Obrazy SEM faz mineralnych obecnych w diatomicie kalcynowanym w temperaturze 1200°C
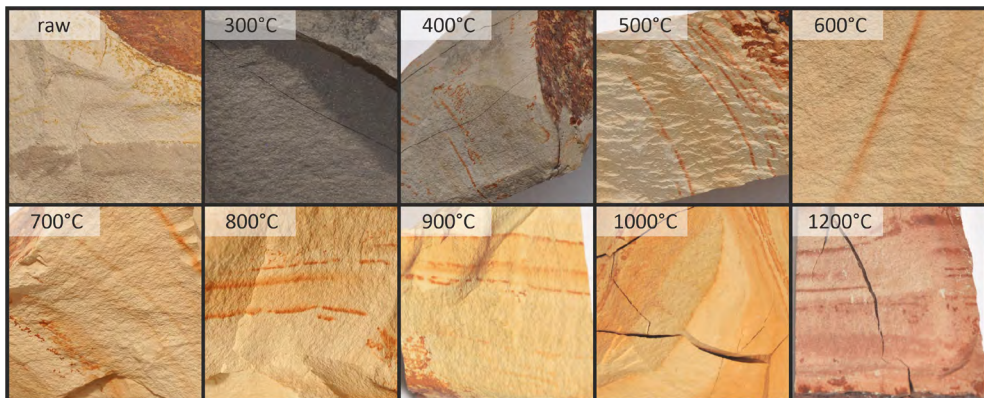

Fig. 11. Macroscopic images of diatomite samples calcined at various temperatures

Rys. 11. Makroskopowe obrazy prób diatomitu kalcynowanych w różnych temperaturach

and 21.31%, respectively, during further calcination. The final water absorption value was therefore half of the initial value, and the open porosity decreased by 1/3 compared to the raw samples. The apparent density of diatomite changed analogously, initially decreasing to 1.27 g/cm^3, and increasing to 1.65 g/cm^3 in the final stages of calcination (Table 3).

The Vickers microhardness, which was approximately 13.5–13.6 MPa for raw samples and samples calcined at 300°C, gradually increased to 85.65 MPa as a result of calcination at subsequent temperatures (Table 3). It should be emphasised that the calcination process caused a linear increase in microhardness in the range of 20–800°C and an exponential increase in the range of 800–1,000°C. Above a temperature of 1,000°C, the HV growth rate was again low (Figure 12).
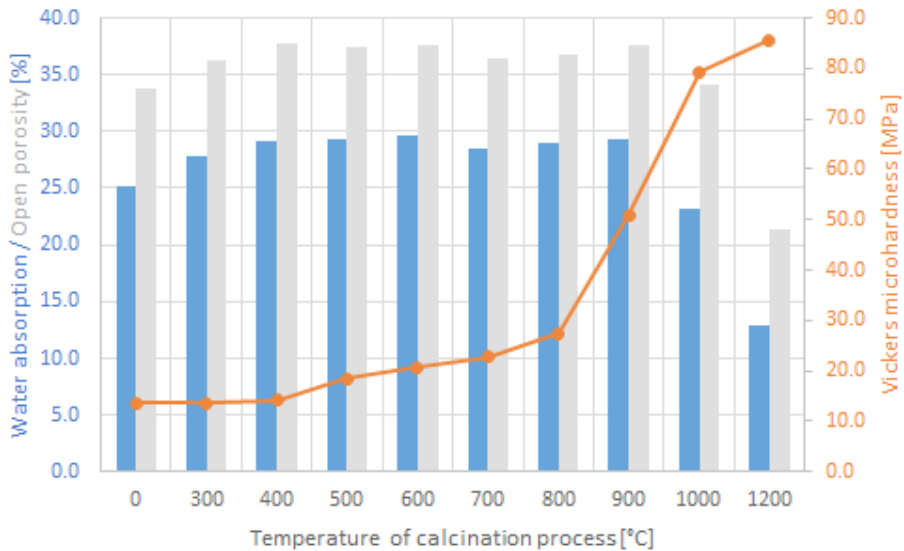
Fig. 12. Changes in water absorption, open porosity and Vickers microhardness depending
on the calcination temperature for diatomite

Rys. 12. Zmiany nasiąkliwości wagowej, otwartej porowatości i mikrotwardości Vickersa
w zależności od temperatury kalcynacji diatomitu

4. Discussion

The results of research and observations have shown that the changes observed in the calcined diatomites occur continuously, while their nature and intensity depend on the calcination temperature. The analysis of this variability allowed the identification of five stages of the calcination process, the limits of which were determined by the effects of transformations of mineral components related to the increasing temperature.

4.1. Stage I (20–400°C)

In this temperature range, mainly endothermic reactions took place in the diatomite. Initially, there was a gradual evaporation of adsorption water, which was also found by other authors in similar studies (Mendioroz et al. 1989; Bolewski and Manecki 1993; Chen et al. 2004; Yılmaz and Ediz 2008; Posi et al. 2014; Zheng et al. 2018). Above a temperature of 100°C, the dehydration process began, affecting opal and clay minerals, which were identified by XRD analysis as illite, kaolinite, and montmorillonite. This process, of an endothermic nature, occurred at temperatures up to approx. 350°C with the main phase

up to approx. 200°C (Figure 2). After exceeding the temperature of 200°C, the exothermic combustion reaction of the organic matter began, which theoretically could last up to a temperature of approximately 500°C (Mendioroz et al. 1989; Zhi-Ying et al. 2009; Ediz et al. 2010; Zheng et al. 2018). In the case of the tested diatomites, this is confirmed by the grey colour of the sample, which persisted up to the calcination temperature of 500°C (Figure 11). The existence of a narrow exothermic effect in the range of 250–400°C on the DTA curve also proves the presence of the discussed process. At a higher temperature (above 400°C), the intensity of endothermic dehydration and subsequent dehydroxylation reactions exceeded the intensity of combustion reactions, which was marked by a significant decrease in the DTA curve.

Both dehydration and combustion led to a mass loss of the rock sample, which occurred mainly in the temperature range of 200–300°C, when both processes took place simultaneously and with the greatest intensity, as evidenced by the TG and DTG curves (see also: Ediz et al. 2010) (Figure 2). By the end of the discussed stage (at 400°C), the sample had lost 7.5% of its initial mass. At the same time, the open porosity of diatomite increased significantly from 33.86% to 37.77% (relative increase of 11.5%) and associated with this water absorption from 25.20% to 29.21% (relative increase of approx. 16%) (Table 3) (see also: Sun et al. 2013). The increase in the water absorption of calcined diatomite should also improve its sorption properties. SEM analysis confirmed an increase in the number and size of pores in the sample calcined at 400°C, compared to the raw diatomite sample. This was observed within the matrix. However, no changes were found in the state of preservation of other rock components. The discussed phenomena did not cause significant changes in Vickers microhardness, which remained unchanged up to a temperature of 300°C, increasing only at the end of this stage (approx. 400°C) by approx. 5% (Table 3).

4.2. Stage II (400–600°C)

As the temperature increased above 400°C, further combustion of organic matter continued. This stage also includes the main phase of dehydroxylation of clay minerals, which leads to a change in the internal structure of these minerals (Stoch 1974). The dehydroxylation process of clay minerals was initiated at temperatures above 400°C in the case of kaolinite, resulting in the formation of metakaolinite, and continued above 500°C for illite and finally for smectites. The co-occurrence of the above processes is marked on the DTA curve as an endothermic effect, lasting up to a temperature of approximately 650°C, although much less intense from a temperature of 500°C (Figure 2). Meanwhile, the XRD curve determined for diatomite calcined at 600°C revealed the disappearance of the peaks corresponding to kaolinite and the weakening of the intensity of those peaks corresponding to illite, muscovite or montmorillonite (Figure 3) (compare: Posi et al. 2014). The discussed processes resulted in a simultaneous loss of sample mass, the rate of which began to decrease significantly from a temperature of approximately 500°C. This moment can be attributed to

the end of combustion and the main stage of dehydration of clay minerals (Mendioroz et al. 1989; Chen et al. 2004; Yilmaz and Ediz 2008; Ediz et al. 2010).

At a temperature of 573°C, the well-known transformation of low α-quartz into high β-quartz took place, which was marked on the DTA curve by a deepening of the endothermic peak. Changing the dimensions of quartz could have led to internal tensions in the grains of this mineral as well as in their surroundings, and consequently to the formation of microcracks (Stoch 1974; Martín-Márquez et al. 2010; Figarska-Warchoł et al. 2019; Johnson et al. 2021). Manifestations of such a phenomenon were found in SEM images (Figure 5B). The process of crack formation and gradual destruction within feldspar grains was also observed (compare: Zhi-Ying et al. 2009) (Figure 6B). Greater resistance was demonstrated by opal diatom shells, the structure of which underwent only minor changes during calcination at 600°C by the formation of small cracks and sometimes widening of the pores inside the diatom frustuli, probably related to the decomposition of some of the organic and clay components. (Figure 4B) (Figarska-Warchoł et al. 2019). The first symptoms of changes in the structure of titanium oxide crystals were found in samples calcined at 600°C. They were expressed by the appearance of cracks. The colour change of the samples from grey to pink with rusty streaks can be attributed to the removal of organic matter and – first of all – the effects of the iron oxidation reactions (Sun et al. 2013) (Figure 11).

At this stage of calcination, minor changes in the rock structure did not lead to a further increase in the open porosity of diatomite, which remained at a stable level of approximately 37%. The phase transformations of minerals had a significant impact on the rock's microhardness. In diatomite calcined at 500°C, the Vickers microhardness increased by over 35% compared to the initial value, and by as much as over 53% at 600°C (Table 3).

4.3. Stage III (600–800°C)

At this stage, the dehydroxylation processes of clay minerals were completed. They last the longest (up to a temperature of approximately 750°C) in the case of smectites (Bolewski and Manecki 1993), the presence of which in the examined diatomite samples was small. This is evidenced by the shape of the DTA curve, which has a straight, flat course in the temperature range of 750–800°C (Figure 2). This was accompanied by a much smaller loss of sample mass than before. Whereas, in the XRD curves of diatomite samples calcined at 700°C and 800°C, further weakening of the peaks corresponding to illite, muscovite, kaolinite, smectites, and alkali feldspars was observed (Figure 3) (compare: Zhi-Ying et al. 2009).

SEM studies showed that the number of cracks occurring in feldspar, quartz, and diatom grains increased with temperature rising. In the case of diatoms, noticeable changes in pore size occurred already at a temperature of 600°C. Their walls were clearly melted at a temperature of 800°C (Figure 4C), which is facilitated by the presence of quite a large amount of alkalis contained in feldspars and clay minerals (compare: Zhi-Ying et al. 2009; Sun et al.

2013; Figarska-Warchoł et al. 2019; Li et al. 2021). However, the general structure of diatoms was still preserved at this stage (compare: Posi et al. 2014).

At a temperature of 700°C, dehydroxylation of glauconite and the subsequent change in its volume led to the formation of cracks around the grains of this mineral, clearly separating them from the surrounding diatoms and matrix components (Figure 9B). At a temperature of 800°C, the formation of iron oxides from glauconite (Figure 9C) as well as iron oxides and titanium oxides from ilmenite began (Figure 7A, 7B) (compare: Mashlan et al. 2012, Simpraditpan et al. 2013; Mehdilo and Irannajad 2021).

The final stages of (1) dehydroxylation of clay minerals, (2) the initial phase of melting of diatoms, and (3) cracks forming in the minerals, which are only an admixture in the composition of diatomite, slightly influenced the porosity of the rock. Initially, in the temperature range of 600–700°C, the open porosity of diatomite decreased from 37.65% to 36.45%, and then – up to the temperature of 800°C – it did not show any significant changes (Table 3). A temperature of 800°C ends the calcination phase in which the microhardness of diatomite increased linearly (Figure 12). After calcination at 700°C, its value was 67% higher, and at 800°C it was 102% higher compared to the raw sample.

4.4. Stage IV (800–1,000°C)

Stage IV of calcination carried out in the temperature range of 800–1,000°C, is associated with significant changes that occur in the structure of some minerals. At a temperature range of approximately 850–900°C, the three-dimensional structure of the anhydrous form of smectites breaks down (Goren et al. 2002). In the case of illite, a similar process occurs at a temperature of approximately 900°C. These endothermic reactions are followed by reorganization of the metakaolinite structure and crystallization of the spinel phase at temperatures of 950–980°C (Stoch 1974). The latter phenomena produce an exothermic effect, as evidenced by the increasingly weaker negative balance of heat exchange with the environment (Figure 2).

On the XRD curve of diatomite calcined at 900°C, the above-described processes were marked by a weakening or disappearance of the peaks corresponding to illite, muscovite, kaolinite, and montmorillonite, which was accompanied by the highest share of amorphous silica (Figure 3). At 1,000°C, there are no peaks corresponding to clay minerals on the XRD curve, while peaks related to hematite and small peaks of metakaolinite appeared. A high content of amorphous silica was also found.

SEM observations revealed that at a temperature of 900°C there were very distinct changes in the internal structure of diatoms by closing some of their pores with silica (Figure 4D). The quartz and feldspar grains were partially melted and quite intensively fractured, probably also as a result of the stresses arising during cooling of the samples (Figure 5C, 6C, 6D). The unmixing of mineral phases in ilmenite led to the destruction of its internal structure and the formation of pores in its grains. (Figure 7C). Micas and glauconite retained their

structure up to the calcination temperature of 900°C, although this temperature influenced the formation of open cracks along the mica cleavage planes (Figure 8B).

The increase in the calcination temperature to 1,000°C resulted in significant intensification of mineral transformations. The structure of the hardly modified Na-feldspars became difficult to identify microscopically, while the K-feldspars melted and became highly porous (Figure 6E). The glauconite grains were completely decomposed, their internal structure became spongy, and only the external contours of the grains were preserved (Figure 9D). The micas were partially disintegrated, which resulted in the formation of iron oxides (Figure 8B).

Iron compounds previously formed at a temperature of 900°C as a result of the transformation of various mineral grains (e.g. mica, glauconite) were oxidised at a temperature of 1,000°C. This led to the formation of hematite, occurring in the form of small clusters scattered in the matrix or emphasising the boundaries of the mineral grains from which they developed (Figure 9D) (compare: Balek and Šubrt 1995; Komraus and Adamczyk 1999; Lewicka 2017). There were significant changes in the internal structure of ilmenite grains, with visible symptoms of demixing of newly formed iron and titanium oxides (Figure 7D) (compare: Alraddadi et al. 2020). In the diffractogram of diatomite calcined at 1,000°C, hematite was the main oxide phase of iron (Figure 3).

It was found that with a total mass loss of the sample of 11%, the open porosity, relatively unchanged up to 900°C, decreased rapidly at 1,000°C to a value of 34.11%, comparable to that of raw diatomite (similarly as it was found in the case of Turkish or Chinese diatomites, see: Yılmaz and Ediz 2008; Zhi-Ying et al. 2009; Ediz et al. 2010; Elmas and Bentli 2013). The water absorption decreased even more and its value dropped to a level lower than the initial one (Table 3). Such a severe decrease in porosity was also observed in clay rocks containing kaolinite, sintered at temperatures above 900°C (Ha et al. 2013). This is promoted by the formation of liquid phases that fill the voids.

Closing the pores with silica as well as the formation of hematite and a small amount of mullite resulted in an exponential increase in the microhardness of diatomite at this stage of calcination (compare: Posi et al. 2014). The value of this parameter at a calcination temperature of 1,000°C increased almost 5 times compared to the initial value determined for the raw sample (Table 3).

4.5. Stage V (1,000–1,200°C)

In the temperature range of 1,000–1,200°C, the process of formation of new mineral phases continued. Cristobalite was formed from the transformation of amorphous silica at a temperature of 1100–1150°C, and mullite came from the decomposition products of clay minerals (Goren et al. 2002; Yilmaz, Ediz 2008; Zhi-Ying et al. 2009; Posi et al. 2013, 2014; Zheng et al. 2018). This is confirmed by the presence of peaks characteristic of these two components in the XRD curve of diatomite calcined at 1,200°C (Figure 3). In the presence

of feldspar admixtures, which act as fluxes due to the alkalis contained in them, a partial transformation of quartz into cristobalite or amorphous silica was also possible (Reka et al. 2015; Li et al. 2021). In the case of the tested diatomites, this would be evidenced by a clear weakening of the quartz peaks in the XRD diagram of diatomite calcined at 1,200°C. Its larger grains visible in SEM images show signs of melting and cracking (Figure 5D). In turn, the authors attribute the increase in the share of the amorphous silica phases to the transformation of quartz, as well as to the decomposition of clay minerals and feldspars (Figure 10A) (compare: Zhi-Ying et al. 2009; Li et al. 2021). The latter process is confirmed by the lack of peaks corresponding to clay minerals and feldspars on the XRD curve for a temperature of 1,200°C (Figure 3).

Relatively weak peaks of mullite about peaks of cristobalite may indicate a kaolinite content below 25%, i.e. lower than estimated based on chemical composition calculations (Tables 1, 2) because only such a proportion of kaolinite favors the formation of mullite (Ha el al. 2013). The calcination temperature in the range of 1,000–1,200°C and the isometric form of mullite crystals visible in SEM images indicate that it is rather a primary mullite (see: Chen et al 2000; Martín-Márquez et al 2010). Needle-like mullite crystals – typical of mature forms of this mineral – in the examined diatomites are formed from the liquid phase as a result of calcination at 1,200°C, occasionally, for example, from the transformation and melting of feldspar crystals (Figure 10B).

The research also showed that most diatoms underwent significant transformation, mainly melting, at this stage of calcination. Only some of them retained shapes similar to the original ones and residual internal porosity (Figure 4E).

SEM observations confirmed that in the discussed calcination stage there was an almost complete breakdown of the structure of minerals such as mica, feldspar, glauconite, and ilmenite (Figure 7E, 9E, 10A). Iron released as a result of the decomposition of the above-mentioned minerals, as well as from the decomposition of clay minerals and iron oxides/hydroxides already present in the matrix, was transformed into hematite. Its share was probably increased up to a temperature of approximately 1,100°C (Kądziołka-Gaweł et al. 2022), after which its partial transformation into other oxides took place (compare: Nurdini et al. 2022). The effect of the latter process is much less intense hematite peaks in the XRD diagram of diatomite exposed to a temperature of 1,200°C (Figure 3). SEM microscopy showed numerous small accumulations of hematite scattered throughout the sample, encrusting especially the pore walls of diatoms (Figure 4F). They also cause a change in the colour of the rock from pink to rusty red (Figure 11) (see: Nurdini et al. 2022).

Calcination performed in this highest temperature range resulted in an extreme reduction in the porosity of the diatomite. Its value decreased to 21.31%, which corresponds to approximately 2/3 of the porosity value of raw diatomite (Table 3). At the same time, the water absorption decreased by half compared to raw diatomite, and its final value was 12.94%. Calcination carried out at a temperature 1,200°C as well as the formation of mullite and cristobalite once again strengthened the rock structure, which was manifested

by a further, although slight, increase in microhardness. Its value after this process was 85.65 MPa and was over five times higher than in raw diatomite. The above result correlates with the compressive strength of calcined Polish diatomites obtained in the research of Kaleta et al. (2007).

Conclusions

The research has shown that during calcination in conditions of increasing temperature, irreversible changes in the mineral composition and structure of the diatomite occurred.

Dehydration of opal and dehydroxylation of clay minerals as well as combustion of organic matter occurring at temperatures below 500°C led to a significant increase in the open porosity of diatomite while improving its hardness. The higher temperature contributed to the formation of cracks in feldspar, quartz, and diatom grains. At a temperature of 800°C, the process of melting of the diatom walls and the disintegration of glauconite and ilmenite began, which resulted in the formation of iron oxides and titanium oxides. These processes slowed down the increase in rock porosity.

Significant changes occurred in diatomites exposed to temperatures up to 1,000°C. The structure of the anhydrous form of smectites then disintegrated, and metakaolinite (later mullite), hematite, and a large amount of the amorphous silica phase were formed. Silica closed a significant part of the pores in the diatoms, and the quartz and feldspar grains were partially melted. This resulted in a significant reduction in the open porosity of the rock and a significant increase in its hardness. These phenomena continued at higher temperatures up to 1,200°C, when the structure of mica, feldspar, glauconite, and ilmenite almost completely disintegrated. This last stage of calcination resulted in a drastic reduction in the open porosity of the diatomite, below the initial value, and a slight subsequent increase in microhardness, which was ultimately five times higher than in raw diatomite.

The presented results indicate that the optimal calcination temperature for the discussed diatomites is 900°C, as it ensures the highest increase in their porosity by 11% and an almost threefold increase in their hardness. Calcination temperatures above 1,000°C, despite the large amount of energy consumption, make it possible to obtain a mechanically resistant material that can be the basis for the production of lightweight aggregates. On the other hand, even a calcination temperature of 400°C, which provides significantly lower process costs, is sufficient to improve sorption properties. The calcination process also changes the chemical composition of diatomite, because as a result of calcination, it is deprived of organic matter, which causes a relative increase in the 1,200 content.

In the Jawornik deposit, several fairly homogeneous lithological complexes can be distinguished, composed of five easily distinguishable varieties of diatomites (Figarska-Warchoł et al. 2015). The occurrence of the studied blocky diatomites in layers several meters thick favours their selective exploitation. The improvement of their technological features as

a result of calcination makes it similar to the best quality varieties of diatomites found in the deposit. Thanks to this, from approximately 80% of the deposit profile it is possible to obtain a raw material of high quality suitable for various applications.

The Authors have no conflicts of interest to declare.

REFERENCES

Alraddadi et al. 2020 – Alraddadi, S., Saeed, A. and Assaedi, H. 2020. Effect of thermal treatment on the structural, electrical, and dielectric properties of volcanic scoria. *Journal of Materials Science: Materials in Electronics* 31(14), pp. 11688–11699, DOI: 10.1007/s10854-020-03720-0.

Balek, V. and Šubrt, J. 1995. Thermal behaviour of iron(III) oxide hydroxides. *Pure and Applied Chemistry* 67(1), pp. 1839–1842, DOI: 10.1351/pac199567111839.

Behl, R.J. 1999. *Since Bramlette* (1946): *The Miocene Monterey Formation of California revisited.* [In:] Moores, E.M., Sloan, D. and Stout, D.L. (eds.). *Classic Cordilleran Concepts: A View from California: Boulder, Colorado, Geological Society of America, Special Paper* 338, DOI: 10.1130/0-8137-2338-8.301.

Bolewski, A. and Manecki, A. 1993. *Detailed mineralogy* (*Mineralogia szczegółowa*). Warszawa: PAE (*in Polish*).

Bradbury, J.P. and Krebs, W.N. 1995. *Fossil continental diatoms: paleolimnology, evolution, and biochronology.* [In:] *Siliceous Microfossils (Short Courses in Paleontology 8).* The Paleontological Society, Knoxville, Tennessee, pp. 119–138, DOI: 10.1017/S2475263000001458.

Chen et al. 2000 – Chen, C.Y., Lan, G.S. and Tuan, W.H. 2000. Preparation of mullite by the reaction sintering of kaolinite and alumina. *Journal of the European Ceramic Society* 20, pp. 2519–2525, DOI: 10.1016/S0955-2219(00)00125-4.

Chen et al. 2004 – Chen, Y.F., Wang, M.C. and Hon, M.H. 2004. Phase transformation and growth of mullite in kaolin ceramics. *Journal of the European Ceramic Society* 24, pp. 2389–2397, DOI: 10.1016/S0955-2219(03)00631-9.

Crangle, R. 2024. *Diatomite*. Mineral Commodity Summaries, January 2024. U.S. Geological Survey.

Ediz et al. 2010 – Ediz, N., Bentli, İ. and Tatar, İ. 2010. Improvement in filtration characteristics of diatomite by calcination. *International Journal of Mineral Processing* 94, pp. 129–134, DOI: 10.1016/j.minpro.2010.02.004.

Elmas, N and Bentli, İ. 2013. Environmental and depositional characteristics of diatomite deposit, Alayunt Neogene Basin (Kutahya), West Anatolia, Turkey. *Environmental Earth Sciences* 68, pp. 395–412, DOI: 10.1007/s12665-012-1745-5.

EN 1936. Natural stone test methods – Determination of real density and apparent density. and of total and open porosity. CEN European Committee for Standarization.

EN 13755. Natural stone test methods – Determination of water absorption at atmospheric pressure. CEN European Committee for Standarization.

Figarska-Warchoł et al. 2015 – Figarska-Warchoł, B., Stańczak, G., Rembiś, M. and Toboła, T. 2015. Diatomaceous rocks of the Jawornik deposit (the Polish Outer Carpathians): petrophysical and petrographical evaluation. *Geology, Geophysics and Environment* 41(4), pp. 311–331, DOI: 10.7494/geol.2015.41.4.311.

Figarska-Warchoł et al. 2019 – Figarska-Warchoł, B., Rembiś, M. and Stańczak, G. 2019. The impact of calcination on changes in the physical and mechanical properties of the diatomites of the Leszczawka Member (the Outer Carpathians, Poland). *Geology, Geophysics and Environment* 45(4), pp. 269–282, DOI: 10.7494/geol.2019.45.4.269.

Flower, R.J. 2013. *Diatom Methods. Diatomites: Their Formation, Distribution, and Uses*. [In:] Elias, S.A. and Mork, C.J. (eds.), *Encyclopedia of Quaternary Science*, Elsevier, Amsterdam, pp. 501–506.

Frings et al. 2014 – Frings, P.J., Clymans, W., Jeppesen, E., Lauridsen, T.L., Struyf, E. and Conley, D.J. 2014. Lack of steady-state in the global biogeochemical Si cycle: emerging evidence from lake Si sequestration. *Biogeochemistry* 117, pp. 255–277, DOI: 10.1007/s10533-013-9944-z.

Goren et al. 2002 – Goren, R., Baykara, T. and Marsoglu, M. 2002. Effects of purification and heat treatment on pore structure and composition of diatomite. *British Ceramic Transactions* 101, pp. 177–180, DOI: 10.1179/096797802225003361.

Ha et al. 2013 – Ha, J.H., Oh, E., Bae, B. and Song, I.H. 2013. The effect of kaolin addition on the characteristics of a sintered diatomite composite support layer for potential microfiltration applications. *Ceramics International* 39, pp. 8955–8962, DOI: 10.1016/j.ceramint.2013.04.092.

Harwood et al. 2007 – Harwood, D.M., Nikolaev, V.A. and Winter, D.M. 2007. Cretaceous records of diatom evolution, radiation, and expansion. *The Paleontological Society Papers* 13, pp. 33–59, DOI: 10.1017/S1089332600001455.

Johnson et al. 2021 – Johnson, S.E., Song, W.J., Cook, A.C. Vel, S.S. and Gerbi, C.C. 2021. The quartz $\alpha \leftrightarrow \beta$ phase transition: Does it drive damage and reaction in continental crust? *Earth and Planetary Science Letters* 553, DOI: 10.1016/j.epsl.2020.116622.

Kaleta et al. 2007 – Kaleta, J., Papciak, D. and Puszkarewicz, A. 2007. Clinoptylolite and diatomite in respect of their usefulness for water conditioning and wastewater purification (*Klinoptylolity i diatomity w aspekcie przydatności w uzdatnianiu wody i oczyszczaniu ścieków*). *Gospodarka Surowcami Mineralnymi – Mineral Resources Management* 23(3), pp. 21–34 (*in Polish*).

Kądziołka-Gaweł et al. 2022 – Kądziołka-Gaweł, M., Wojtyniak, M. and Klimontko, J. 2022. High temperature transformation of iron-bearing minerals in basalt: Mössbauer spectroscopy studies. *Mineralogia* 53, pp. 10–19, DOI: 10.2478/mipo-2022-0002.

Komraus, J.L. and Adamczyk, Z. 1999. Transformations of iron minerals during thermal processing of Tertiary basalt from the Jawor region (*Przemiany minerałów żelaza podczas obróbki termicznej trzeciorzędowego bazaltu rejonu Jawora*). *Physicochemical Problems of Mineral Processing* 33(1), pp. 73–82 (*in Polish*).

Kotlarczyk, J. 1966. Diatomite horizon from the Krosno beds against the background of the geological structure of the Skole unit in the Polish Carpathians (*Poziom diatomitowy z warstw krośnieńskich na tle budowy geologicznej jednostki skolskiej w Karpatach polskich*). *Studia Geologica Polonica*. 19. Warszawa: Wyd. Geologiczne (*in Polish*).

Kotlarczyk, J. 1982. The role of diatoms in sedimentation and biostratigraphy of the Polish Flysch Carpathians. *Acta Geologica Academiae Scientiarum Hungaricae* 25(1–2), pp. 9–21.

Kotlarczyk, J. 1988a. *Jawornik Ruski – kopalnia diatomitu. Poziom diatomitów z Leszczawki, najmłodsza olistostroma we fliszu*. [In:] Kotlarczyk J., Pękala K. and Gucik S. (eds.), *Karpaty Przemyskie. Przewodnik 59 Zjazdu Polskiego Towarzystwa Geologicznego*, Przemyśl, 16–18 września 1988, Kraków: AGH, pp. 115–118 (*in Polish*).

Kotlarczyk, J. 1988b. Level of diatomites from Leszczawka. Point B-3. Russian Jawornik. 1. Geology and properties of the raw material (*Poziom diatomitów z Leszczawki. Punkt B-3. Jawornik Ruski. 1. Geologia i własności surowca*). [In:] Kotlarczyk J., Pękala K. and Gucik S. (eds.), *Karpaty Przemyskie. Przewodnik 59 Zjazdu Polskiego Towarzystwa Geologicznego*, Przemyśl, 16–18 września 1988, Kraków: AGH, pp. 149–154 (*in Polish*).

Kotlarczyk, J. 2008. *Diatomites* (*Diatomity*). [In:] Kłapyta Z. and Żabiński W. 2008. (eds.) *Polish mineral sorbents* (*Sorbenty mineralne Polski*). Kraków: Uczelniane Wydawnictwa Naukowo-Dydaktyczne (*in Polish*).

Kotlarczyk et al. 1986 – Kotlarczyk, J., Brożek, M. and Michalski, M. 1986. Diatomites of the Polish Carpathians – occurrence, quality, processing and applications (*Diatomity polskich Karpat – występowanie, jakość, przeróbka i zastosowania*). *Gospodarka Surowcami Mineralnymi – Mineral Resources Management* 2(3–4), pp. 497–523 (*in Polish*).

Kotlarczyk et al. 1987 – Kotlarczyk J. and Kaczmarska I. 1987. Two diatoms horizons in the Oligocene and (?) Lower Miocene of the Polish Outer Carpathians. *Annales Societatis Geologorum Poloniae* 57, pp. 143–188.

Koszarski, L. and Żytko, K. 1961. Jasło Shales within the Menilite-Krosno Series in the Middle Carpathians. *Biuletyn Instytutu Geologicznego* 166, pp. 87–232.

Lewicka, E. 2017. Phase transitions of ferruginous minerals in the course of thermal processing of feldspar-quartz raw materials from the Sobótka region (Lower Silesia). *Gospodarka Surowcami Mineralnymi – Mineral Resources Management* 33(1), pp. 93–110, DOI: 10.1515/gospo-2017-0010.

Li et al. 2021 – Li, W., Xu, C., Xie, A., Chen, K, Yang, Y., Liu, L. and Zhu, S. 2021. Microstructure study of pha-se transformation of quartz in potassium silicate glass at 900°C and 1,000°C. *Crystals* 11, DOI: 10.3390/cryst11121481.

Malata, T. and Poprawa, P. 2006. *Evolution of the Skola subbasin* (*Ewolucja subbasenu skolskiego*). [In:] Oszczyp-ko N., Uchman A. and Malata E. (eds.), *Paleotectonic development of the outer Carpathian basins and the Pieniny Rock Belt* (*Rozwój paleotektoniczny basenów Karpat zewnętrznych i pienińskiego pasa skałkowego*). Kraków: UJ, pp. 103–110 (*in Polish*).

Marczyk et al. 2022 – Marczyk, J., Pławecka, K., Hebdowska-Krupa, M., Nykiel, M. and Łach, M. 2022. Research on diatomite from Polish deposits and the possibilities of its use. *Journal of Achievements in Materials and Manufacturing Engineering* 115(1), pp. 5–15, DOI: 10.5604/01.3001.0016.2337.

Martín-Márquez et al. 2010 – Martín-Márquez, J., Rincón, J.M. and Romero, M. 2010. Mullite development on firing in porcelain stoneware bodies. *Journal of the European Cearmic Society* 30, pp. 1599–1607, DOI: 10.1016/j.jeurceramsoc.2010.01.002.

Mashlan et al. 2012 – Mashlan, M., Martinec, P., Kašlík, J., Kovářová, E. and Scucka, J. 2012. Mössbauer study of transformation of the cations during thermal treatment of glauconite in air. *AIP Conference Proceedings* 1489, pp. 169–173, DOI: 10.1063/1.4759486.

Mehdilo, A. and Irannajad, M. 2021. Surface modification of ilmenite and its accompanied gangue minerals by thermal pretreatment: Application in flotation process. *Transactions of Nonferrous Metals Society of China* 31, pp. 2836–2851, DOI: 10.1016/S1003-6326(21)65697-2.

Mendioroz et al. 1989 – Mendioroz, S., Belzunce, M.J. and Pajares, J.A. 1989. Thermogravimetric study of diatomi-tes. *Journal of Thermal Analysis* 35, pp. 2097–2104, DOI: 10.1007/BF01911874.

Nurdini et al. 2022 – Nurdini, N., Ilmi, M.M., Maryanti, E., Setiawan, P., Kadja, G.T.M. and Ismunandar, 2022. Thermally-induced color transformation of hematite: insight into the prehistoric natural pigment preparation. *Heliyon* 8, DOI: 10.1016/j.heliyon.2022.e10377.

Opfergelt et al. 2011 – Opfergelt, S., Eiriksdottir, E.S., Burton, K.W., Einarsson, A., Siebert, C., Gislason, S.R. and Halliday, A.N. 2011. Quantifying the impact of freshwater diatom productivity on silicon isotopes and silicon fluxes: Lake Myvatn, Iceland. *Earth and Planetary Science Letters* 305, pp. 73–82, DOI: 10.1016/j.epsl.2011.02.043.

Oszczypko, N. 2008. *Outher Carpathians in Poland*. [In:] McCann T. (ed), *The geology of Central Europe*. Vol. 2: *Mesozoic and Cenozoic*. London: Geological Society, pp. 1078–1081.

Plunkett et al. 2004 – Plunkett, G.M., Whitehouse, N.J., Hall, V.A., Brown, D.M. and Baillie, M.G.L. 2004. A pre-cisely-dated lake-level rise marked by diatomite formation in northeastern Ireland. *Journal of Quaternary Science* 19, pp. 3–7, DOI: 10.1002/jqs.816.

Posi et al. 2013 – Posi, P., Lertnimoolchai, S., Sata, V. and Chindaprasirt, P. 2013. Pressed lightweight concrete con-taining calcined diatomite aggregate. *Construction and Building Materials* 47, pp. 896–901, DOI: 10.1016/j.conbuildmat.2013.05.094.

Posi et al. 2014 – Posi, P., Lertnimoolchai, S., Sata, V., Phoo-ngernkham, T. and Chindaprasirt, P. 2014. Investigation of properties of lightweight concrete with calcined diatomite aggregate. *KSCE Journal of Civil Engineering* 18(5), pp. 1429–1435, DOI: 10.1007/s12205-014-0637-5.

Reka et al. 2015 – Reka, A.A., Pavlovski, B., Anovski, T., Bogoevski, S. and Boškovski, B. 2015. Phase transforma-tions of amorphous 1,200 in diatomite at temperature range of 1,000–1,200°C. *Geologica Macedonica* 29(1), pp. 87–92.

Russocki ,Z. 1981. *Variability of diatomites in the Leszczawka deposit* (*Zmienność diatomitów w złożu Lesz-czawka*). [In:] Szymańska, A. (ed.), *New directions of application of Polish diatomites in the national eco-nomy: scientific and technical conference* (*Nowe kierunki zastosowań diatomitów polskich w gospodarce narodowej: konferencja naukowo-techniczna*), Przemyśl, 23–24 maja 1980, Warszawa: Wyd. Geologiczne, pp. 30–40.

Simpraditpan et al. 2013 – Simpraditpan, A., Wirunmongkol, T., Pavasupree, S. and Pecharapa, W. 2013. Effect of calcination temperature on structural and photocatalyst properties of nanofibers prepared from low-cost natu-ral mineral by simple hydrothermal method. *Material Research Bulletin* 48, pp. 3211–3217, DOI: 10.1016/j.materresbull.2013.04.083.

Smirnov et al. 2017 – Smirnov, P.V., Konstantinov, A.O. and Gursky, H.J. 2017. Petrology and industrial application of main diatomite deposits in the Transuralian region (Russian Federation). *Environmental Earth Sciences* 76, DOI: 10.1007%2Fs12665-017-7037-3.

Stoch, L. 1974. *Clay minerals* (*Minerały ilaste*). Warszawa: Wyd: Geologiczne (*in Polish*).

Sun et al. 2013 – Sun, Z., Zhang, Y., Zheng, S., Park, Y. and Frost, R.L. 2013. Preparation and thermal energy storage properties of paraffin/calcined diatomite composites as form-stable phase change materials. *Thermochimica Acta* 558, pp. 16–21, DOI: 10.1016/j.tca.2013.02.005.

Szydło et al. 2014 – Szydło, A., Garecka, M., Jankowski, L. and Malata, T. 2014. Paleogene microfossils from the submarine debris flows in the Skole Basin (Polish and Ukraine Outer Carpathians). *Geology, Geophysics and Environment* 40(1), pp. 49–65, DOI: 10.7494/geol.2014.40.1.49-65.

Vassileva et al. 2011 – Vassileva, P., Gentscheva, G., Ivanova, E., Tzvetkova, P., Voykova, D. and Apostolova, M. 2011. Characterization of natural diatomites from Bulgaria. *Comptes rendus de l'Acad´emie bulgare des Sciences* 64(6), pp. 823–830.

Vassileva et al. 2013 – Vassileva, P., Apostolova, M., Detchev, A. and Ivanova, E. 2013. Bulgarian natural diatomites: modification and characterization. *Chemical Papers* 67(3), pp. 342–349, DOI: 10.2478/s11696-012-0272-x.

Yılmaz, B. and Ediz, N. 2008. The use of raw and calcined diatomite in cement production. *Cement and Concrete Composites* 30, pp. 202–211, DOI: 10.1016/j.cemconcomp.2007.08.003.

Zahradník et al. 2019 – Zahradník, J., Jirásek, J., Zahradník, J. and Sivek, M. 2019. Development of the diatomite production, reserves and its processing in the Czech Republic in 1999–2018. *Gospodarka Surowcami Mineralnymi – Mineral Resources Management* 35(2), pp. 31–48, DOI: 10.24425/gsm.2019.128515.

Zheng et al. 2018 – Zheng, R., Ren, Z., Gao, H., Zhang, A. and Bian, Z. 2018. Effects of calcination on silica phase transition in diatomite. *Journal of Alloys and Compounds* 757, pp. 364–371, DOI: 10.1016/j.jallcom.2018.05.010.

Zhi-Ying et al. 2009 – Zhi-Ying, W., Li-Pang, Z. and Yu-Xiang, Y. 2009. Structural investigation of some important Chinese diatomites. *Glass Physics and Chemistry* 35(6), pp. 673–679, DOI: 10.1134/S1087659609060182.

**TRANSFORMATIONS OF DIATOMITE COMPONENTS AND CHANGES
IN ITS TECHNICAL PROPERTIES CAUSED BY CALCINATION AT DIFFERENT TEMPERATURES –
A CASE STUDY OF THE JAWORNIK DEPOSIT, POLAND**

K e y w o r d s

diatomite, thermal treatment, X-ray diffraction, SEM, Vickers microhardness

A b s t r a c t

Diatomite rocks from the eastern part of the Polish outer Carpathians come in several varieties with different colour, compactness, amount of clay and sandy substance as well as the degree of silicification. One of them is dark grey blocky diatomite, present in the Jawornik deposit and characterised by average quality. During the tests, it was thermally calcined at temperatures from 300°C to 1,200°C in order to improve its functional properties. The results of observations regarding the changes that the rock and its components underwent under conditions of increasing temperature were presented. The results of thermal analysis, X-ray diffraction and tests of physical properties (i.e. density, water absorption and Vickers microhardness) of the rock were presented. Detailed observations of the rock's mineral components were made using a scanning microscope. Their physical changes (e.g. cracks or signs of melting) and chemical transformations were described. It has been shown that during

calcination, irreversible changes occur in the mineral composition and structure of diatomite. It was proven that for the discussed diatomite the optimal calcination temperature is 900°C, as it ensures the greatest increase in its open porosity by 11% and an almost threefold increase in its hardness. The chemical composition of diatomite also changes due to the combustion of the organic matter present in it and the resulting relative increase in the 1,200 content. Calcination improves the technological features of this variety of diatomite, making it similar to the best quality varieties found in this deposit.

PRZEOBRAŻENIA SKŁADNIKÓW DIATOMITU I ZMIANY
JEGO WŁAŚCIWOŚCI TECHNICZNYCH SPOWODOWANE KALCYNACJĄ
W RÓŻNYCH TEMPERATURACH – NA PRZYKŁADZIE ZŁOŻA JAWORNIK, POLSKA

Słowa kluczowe

diatomit, obróbka cieplna, dyfrakcja rentgenowska, SEM, mikrotwardość Vickersa

Streszczenie

Skały diatomitowe pochodzące ze wschodniej części polskich Karpat zewnętrznych występują w kilku odmianach o różnej barwie, zwięzłości, stopniu zailenia, zapiaszczenia i skrzemionkowania. Jedną z nich jest ciemnoszary diatomit o blocznym rozpadzie, powszechnie występujący w złożu Jawornik i reprezentujący tu surowiec o przeciętnej jakości. W trakcie badań został on poddany termicznej kalcynacji w temperaturach od 300 do 1200°C w celu poprawy jego właściwości użytkowych. Przedstawiono wyniki obserwacji i badań dotyczących zmian, jakim ulegała skała i jej składniki w warunkach wzrastającej temperatury. Zaprezentowano wyniki analizy termicznej, dyfrakcji rentgenowskiej i badań właściwości fizycznych (tj. gęstość, nasiąkliwość wodna czy mikrotwardość Vickersa) skały. Przeprowadzono szczegółowe obserwacje w mikroskopie skaningowym składników mineralnych skały. Opisano ich fizyczne zmiany (np. spękania czy oznaki nadtopienie) oraz chemiczne przeobrażenia. Wykazano, że podczas kalcynacji doszło do nieodwracalnych zmian w składzie mineralnym i strukturze diatomitu. Dowiedziono, że dla omawianego diatomitu optymalna temperatura kalcynacji wynosi 900°C, gdyż zapewnia ona największy wzrost jego porowatości o 11% i prawie trzykrotny wzrost jego twardości. Zmianie ulega także skład chemiczny diatomitu na skutek spalenia występującej w nim materii organicznej i wynikającego stąd względnego wzrostu zawartości 1200. Kalcynacja doprowadza do poprawy cech technologicznych tej odmiany diatomitu, upodabniając go do najlepszych jakościowo odmian występujących w złożu.